ChemComm
Chemical Communications

Accepted Manuscript

This article can be cited before page numbers have been issued, to do this please use: S. Yang, J. Zhao, X. Nie, X. Zheng, X. Xie, X. Zheng, H. Fu, H. Chen, R. Li, W. Xue and J. Xu, *Chem. Commun.*, 2025, DOI: 10.1039/D5CC04457J.

ROYAL SOCIETY OF CHEMISTRY

rsc.li/chemcomm

ChemComm

View Article Online
DOI: 10.1039/D5CC04457J

COMMUNICATION

A Tandem Electrocatalysis and Hydroformylation Approach to Synthesize High-Carbon Aldehydes from CO_2

Received 00th January 20xx,
Accepted 00th January 20xx

DOI: 10.1039/x0xx00000x

Siheng Yang,[a] Jiangui Zhao,[a] Xufeng Nie,[b] Xuan Zheng,[a] Xiaobin Xie,[a] Xueli Zheng,[a] Haiyan Fu,[a] Hua Chen,[a] Ruixiang Li,[a] Weichao Xue,[a,*] Jiaqi Xu[a,c,d,*]

The electrochemical CO_2 reduction reaction (eCO_2RR) typically yields low-carbon products (C_n, n≤3), thereby limiting its application scope. Herein, we design a cascaded eCO_2RR-hydroformylation system for synthesizing high-carbon (C_9) aldehydes from CO_2. Ni_xCo_{1-x}@NCNT catalysts enable the production of syngas with a tunable H_2/CO ratio ranging from 0 to 5.3 using CO_2 and H_2O as feedstocks. Subsequently, Rh-based complexes are constructed to catalyze the downstream phenylacetylene hydroformylation. As a result, this tandem electrocatalysis-hydroformylation approach achieves a high phenylacetylene conversion efficiency of 87%, with aldehyde selectivity up to 53% under room pressure and temperature.

The overuse of fossil fuels has resulted in the emission of large amount carbon dioxide (CO_2), causing severe ecological and environmental issues.[1] Electrochemical CO_2 reduction reaction (eCO_2RR) represents one of the promising approaches for mitigating atmospheric CO_2 levels.[2] Although a variety of valuable products can be produced from eCO_2RR now, most are limited to low-carbon compounds (C_n, n≤3), thereby restricting their practical application scope. Luckily, eCO_2RR can produce syngas, a mixture of carbon monoxide (CO) and hydrogen (H_2), which serves as the feedstock of high-carbon compounds.[3]

The syngas with different CO/H_2 ratios can be used for producing different downstream chemicals. For instance, a H_2/CO ratio of 2:1 is suitable for Fischer-Tropsch synthesis to obtain hydrocarbon compounds (e.g., linear α-olefin), while the ratio of 1:1 is favorable for hydroformylation reaction of alkenes or alkynes to produce aldehydes.[4] Thus, to make eCO_2RR technology more practical, efficiently modulating the H_2/CO ratio in the syngas is necessary. To this end, single-atom strategy, alloying strategy, and element-doping strategy have been developed.[5] Nevertheless, producing syngas with H_2/CO ratios that meet industrial requirements under a high current density remains a big challenge.[5a,6] Moreover, hindered by poor production efficiency, reports on the direct utilization of syngas produced via eCO_2RR is also scarce.[7] Hence, it is urgent to develop eCO_2RR catalysts capable of efficiently producing syngas that can be directly utilized in the following synthesis of fine chemicals.

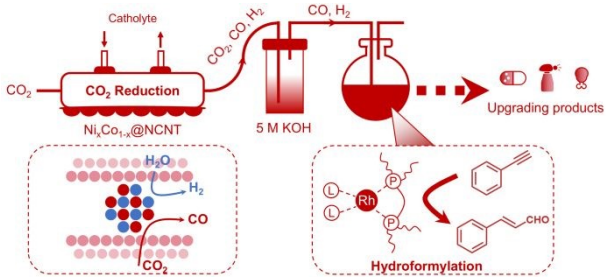

Fig. 1 Schematic illustration of the eCO_2RR-hydroformylation cascaded conversion system to synthesize high-carbon aldehydes from CO_2.

In this work, nitrogen-doped carbon nanotube (NCNT)-coated NiCo alloy catalysts (Ni_xCo_{1-x}@NCNT, where x represents the Ni/(Ni + Co) molar ratio in the raw materials; x = 0.00, 0.15, 0.20, 0.50, and 1.00) are synthesized. These catalysts enable efficient syngas production with adjustable H_2/CO ratio in a total Faradaic efficiency (FE) of ca. 100% under current densities ranging from 100 to 400 mA cm^{-2}. Among the Ni_xCo_{1-x}@NCNT catalysts, $Ni_{0.20}Co_{0.80}$@NCNT exhibits optimal performance, producing syngas with an H_2/CO ratio of ca. 1.64 at 100 mA cm^{-2}, which is well-suited for hydroformylation reactions. Leveraging Rh-based catalysts functionalized with indolybiphosphoramidite ligands developed by our group,[4f] we further construct a tandem eCO_2RR-hydroformylation system

[a] Key Laboratory of Green Chemistry & Technology, Ministry of Education, College of Chemistry, Analytical & Testing Center, Sichuan University, Sichuan 610064, China. Email: weichaoxue@scu.edu.cn
[b] School of Pharmacy, North Sichuan Medical College, Nanchong 637000, PR China.
[c] State Key Laboratory of Oil and Gas Reservoir Geology and Exploitation, School of New Energy and Materials, Southwest Petroleum University, Chengdu 610500, China
[d] Laboratory of Photonics and Interfaces, École Polytechnique Fédérale de Lausanne, 1015 Lausanne, Switzerland. Email: jiaqi.xu@epfl.ch
† Supplementary Information available. See DOI: 10.1039/x0xx00000x

that can directly utilize eCO_2RR-derived syngas for aryl alkyne hydroformylation, enabling the efficient synthesis of high-carbon aldehydes under room pressure and temperature (Fig. 1).

The Ni_xCo_{1-x}@NCNT catalysts were prepared by a facile pyrolysis method. As confirmed by X-ray diffraction (XRD) patterns (Fig. 2A), the as-synthesized catalysts are composed of carbon and metal nanoparticles (NPs). The similar lattice constants and crystal structures of Ni and Co NPs facilitate the formation of NiCo alloy. Along the increasing of Ni content in Ni_xCo_{1-x}@NCNT catalysts, XRD patterns showed a gradual positive shift in the diffraction peaks corresponding to the (111) and the (200) planes of the metal NPs, confirming the formation of NiCo alloys. Moreover, taking $Ni_{0.50}Co_{0.50}$@NCNT catalyst as an example, X-ray photoelectron spectra (XPS, Fig. 2B, C) revealed that compared to Co@NCNT and Ni@NCNT, the Co 2p binding energy in the $Ni_{0.50}Co_{0.50}$@NCNT increased, while the Ni 2p binding energy reduced. This suggested the electron transfer from Co to Ni atoms in the $Ni_{0.50}Co_{0.50}$@NCNT. Moreover, N element was detected in the Ni_xCo_{1-x}@NCNT samples, and metal-N bond, pyridinic N, pyrrolic N, graphitic N and oxidized N species were observed in the N 1s spectra of the samples[8], which suggested the N-doping in the CNT and an interaction between the N sites and the metal NPs (Fig. S1-S3). This interaction can induce the formation of carbon-coated metallic nanoparticles (NPs).[9] Scanning electron microscopy (SEM) and transmission electron microscopy (TEM) images demonstrated that the metal NPs were embedded into the bamboo-like nanotubes (Fig. 2D, E and Fig. S4). High-resolution TEM (HRTEM) images displayed interplanar spacings of 0.34, 0.17, and 0.20 nm, corresponding to the (002) plane of carbon (PDF#04-007-8496), and the (200) and (111) planes of $Ni_{0.50}Co_{0.50}$ alloy (PDF#04-004-8490) (Fig. 2F, G). Then, high-angle annular dark-field scanning transmission electron microscopy (HAADF-STEM) and the corresponding elemental mapping images reveal that nitrogen is uniformly distributed within the carbon nanotubes (CNTs). Additionally, Ni and Co elements are uniformly and co-located within the metal nanoparticles, further supporting the formation of NiCo alloy (Fig. 2H-L and Fig. S5). Similar results were also observed for the $Ni_{0.20}Co_{0.80}$NCNT catalyst (Fig. S6), indicating common structural features among these Ni_xCo_{1-x}NCNT catalysts. Furthermore, as revealed in HAADF-STEM images, no Co or Ni single atom was observed in the catalysts (Fig. S7), which excluded the possibility of single- or dual- atom catalysis. Collectively, all the characterizations above confirmed the successfully synthesis of the Ni_xCo_{1-x}@NCNT catalysts.

The eCO_2RR performance of Ni_xCo_{1-x}@NCNT catalysts was evaluated in a flow cell. It was found that pure cobalt metal exhibited negligible eCO_2RR activity, with a H_2 FE exceeding 99% (Fig. S8). In contrast, Co@NCNT possessed enhanced eCO_2RR activity, with a CO FE (FE_{CO}) of ca. 27%. Additionally, compared to Co@NCNT, the FE_{CO} over Co@NCNT-etch, prepared by soaking Co@NCNT into 6 M HCl solution, reduced from 27% to 7% (Fig. S8), demonstrating that the CO_2RR activity is also relevant to Co content. Thus, these results verified the real catalytic sites for eCO_2RR in the Ni_xCo_{1-x}@NCNT catalysts are the NCNT-coated metal NPs, specifically the interfaces between the

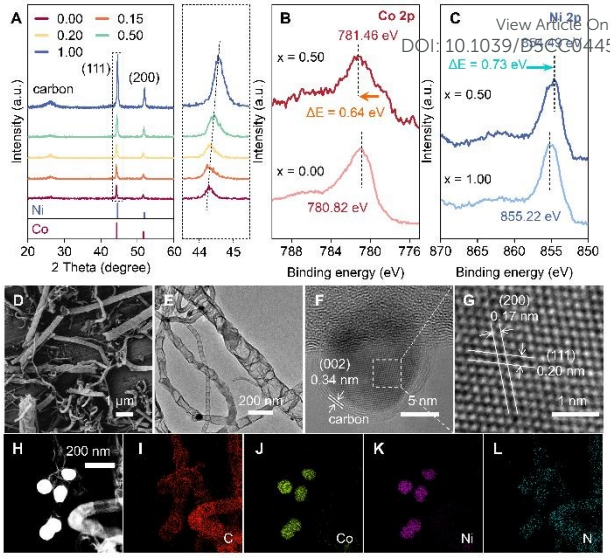

Fig. 2 (A) XRD patterns of Ni_xCo_{1-x}@NCNT, where x represents the Ni/(Ni + Co) molar ratio in the raw materials (x = 0.00, 0.15, 0.20, 0.50, and 1.00). (B) Co 2p XPS spectra of Co@NCNT and $Ni_{0.50}Co_{0.50}$@NCNT. (C) Ni 2p XPS spectra of Ni@NCNT and $Ni_{0.50}Co_{0.50}$@NCNT. (D) SEM image, (E) TEM image, (F, G) HRTEM image, (H) HAADF-STEM image and (I-L) the corresponding elemental mapping images of $Ni_{0.50}Co_{0.50}$@NCNT.

carbon layer and the metal NPs, rather than the pure metal sites or the bare NCNTs. The special three-dimensional structure of the NCNTs was conducive to confine the CO_2 and/or the reaction intermediates within the nanotubes, thereby reinforcing CO_2 activation. This spatial confinement effect likely contributes to the enhanced eCO_2RR activity.[10] Furthermore, the doped N in CNTs can also promote eCO_2RR by enhancing interfacial basicity (especially, pyridinic N) and facilitating charge mobility (e.g., graphitic N).[6a,11] Moreover, with increasing Ni content in the Ni_xCo_{1-x}@NCNT catalysts, the hydrogen evolution reaction (HER) was further inhibited, while the FE_{CO} increased accordingly (Fig. 3A-3B). Notably, the FE_{CO} over Ni@NCNT maintained ca. 99% even under an industrial level current density of 400 mA cm^{-2}, demonstrating its excellent selectivity towards CO. Furthermore, the ^{13}C-labelling experiment captured the *m/z* signal of 29, verifying that the CO was originated from the eCO_2RR process (Fig. S9). The electrochemical impedance spectroscopy (EIS) measurement indicated the interfacial charge transfer efficiency of the cathodic catalysts was reinforced by increasing the Ni content (Fig. S10), thereby enhancing the eCO_2RR activity. Additionally, the electrochemically active surface area (ECSA) measurements showed that the ECSA of the Ni_xCo_{1-x}@NCNT catalyst was also enlarged with the increasing of Ni content (Fig. S11, Table S1), which provided more active sites for CO_2 adsorption and activation. As shown in Table S1, Ni@NCNT possessed a 5.5-fold larger ECSA (24.8 cm^2) than Co@NCNT (4.5 cm^2). Typically, the lattice defects in the CNTs correspond to the D band, whereas the G band arises from the in-plane vibration of sp^2 carbon atoms.[12] The intensity ratios of D band (ca. 1366 cm^{-1})/G band (ca. 1593 cm^{-1}) (I_D/I_G) in the Raman spectra of the three typical samples reflect the disorder degree in their carbon structures, where higher the ratio indicates more defects.[5c,6a] As shown in Fig. S11, in contrast to Ni@NCNT (1.02) or Co@NCNT (0.83),

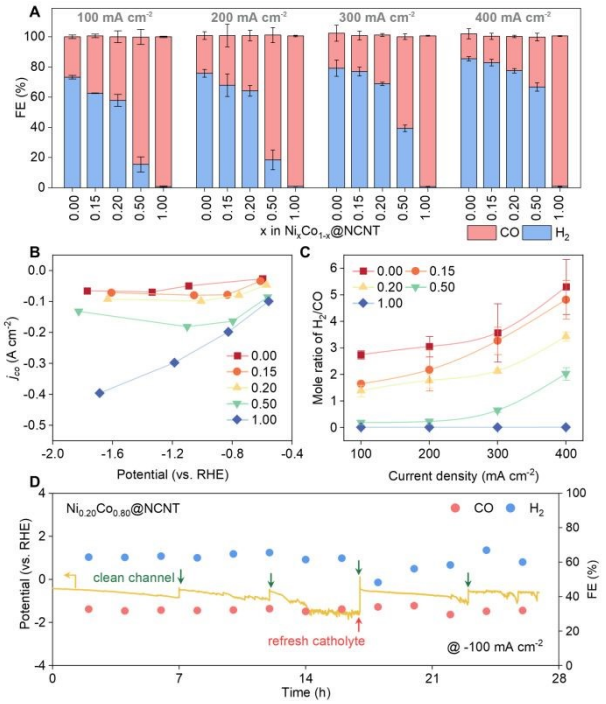

Fig. 3 (A) The eCO_2RR performance, (B) the partial current density of CO, and (C) the corresponding H_2/CO ratios over Ni_xCo_{1-x}@NCNT under different current densities in 1 M KOH solution. (D) The durability of $Ni_{0.20}Co_{0.80}$@NCNT at 100 mA cm^{-2}. Positions indicated by green and red arrows represent the gas channel cleaning and the catholyte refreshing. Error bars in A and C derived from 3 independent replicate experiments.

$Ni_{0.50}Co_{0.50}$@NCNT exhibited a little higher value of I_D/I_G (1.17), indicating the formation of NiCo alloy increased the defects of the CNT. Thus, the defects in the CNTs may not account for the difference in CO selectivity. According to previous work, the adsorption of active hydrogen species (*H) on Co sites is stronger than that on Ni sites, indicating that the HER is more favorable on Co sites compared to Ni sites.[5b,13] Overall, tuning the Ni content in the NiCo alloy plays a critical role in regulating the product selectivity during the eCO_2RR process. Furthermore, the H_2/CO molar ratio can also be adjusted by varying the applied current density. At high current densities, CO_2 mass transfer becomes limited, which inhibits the eCO_2RR activity and favors the HER on Co sites. As a result, the Ni_xCo_{1-x}@NCNT-based systems enable tunable H_2/CO ratios ranging from 0 to 5.3 by regulating the Ni content and the current density (Fig. 3C). Then, the durability of the Ni_xCo_{1-x}@NCNT catalysts was further elucidated at 100 mA cm^{-2}. For example, as depicted in Fig. 3D, the eCO_2RR activity of $Ni_{0.20}Co_{0.80}$@NCNT maintained stable for at least 26 h, delivering an average H_2/CO ratio of ca. 1.64. Fig. S13 displayed that there was no obvious change in the composition and morphology of $Ni_{0.20}Co_{0.80}$@NCNT. To ensure long-term operation, the gas flow channel was cleaned every 6-7 h to mitigate carbonate problem.[14] Besides, the rest Ni_xCo_{1-x}@NCNT catalysts also exhibited excellent stability under 100 mA cm^{-2}, with the H_2/CO ratio remaining nearly unchanged within 5 h (Fig. S14), which indicated their promising potential for future practical applications.

With the Ni_xCo_{1-x}@NCNT-based electrocatalysts enabling efficient syngas generation with adjustable H_2/CO ratios (0 to 5.3), we established a tandem system by coupling eCO_2RR with phenylacetylene hydroformylation to produce high-carbon aldehydes. To ensure an efficient hydroformylation of phenylacetylene at ambient pressure, diphosphine ligands (**L1**-**L3**) were first screened based on our previous report (Fig. 4A).[4f] Initially, to ensure a high conversion of phenylacetylene, a relatively high temperature of 50 °C was set for the hydroformylation reaction. During the hydroformylation of phenylacetylene (Fig. 4B), phenylacetylene could either be hydrogenated into styrene (**a**) or undergo hydroformylation to generate unsaturated neo- or iso-aldehydes (**b** or **c**). Meanwhile, the **b** and **c** could be further hydrogenated to yield corresponding saturated aldehydes (**bH** and **cH**). To evaluate the performance of the eCO_2RR-hydroformylation system, $Ni_{0.20}Co_{0.80}$@NCNT was selected for the electroreduction of CO_2 and H_2O into syngas with a suitable H_2/CO ratio (ca. 1.64), while ligands **L1**-**L3** were screened for the following hydroformylation step. As shown in Fig. 4C, no phenylacetylene conversion was observed when using the commercial ligand **L1**. In contrast, the indolybiphosphoramidite ligands (**L2** and **L3**) developed by our group effectively catalyzed the hydroformylation of phenylacetylene, achieving a phenylacetylene conversion up to ca. 100% under 50 °C after 19 h. Unfortunately, due to the competitive hydrogenation of phenylacetylene, the hydrogenated product **a** was the main product. Among these ligands, **L3** exhibited the highest selectivity towards aldehyde. Low temperature was beneficial for inhibiting the competitive hydrogenation reaction, so ligand **L3** was chosen for the tandem

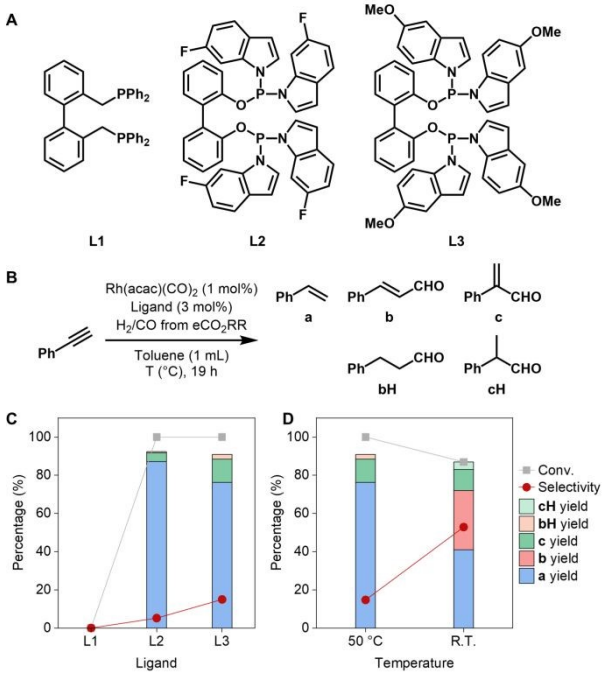

Fig. 4 (A) The phosphine ligands used for phenylacetylene hydroformylation. (B) The reaction formula for phenylacetylene hydroformylation. (C) The performance of the eCO_2RR-hydroformylation system based on the different ligands, where the $Ni_{0.20}Co_{0.80}$@NCNT was used for eCO_2RR with a current density of 100 mA cm^{-2}, and the reaction temperature for the hydroformylation was 50 °C. (D) The effect of temperature on the cascaded hydroformylation reaction based on 2,2'-bis((bis(5-methoxy-1H-indol-1-yl)phosphaneyl)oxy)-1,1'-biphenyl (**L3**), where room temperature (R. T.) is 22 ± 5 °C. The grey points in (C) and (D) represent the conversion of phenylacetylene, while the red points represent the aldehyde selectivity. The yields for the products were determined by gas chromatography (GC).

hydroformylation performance investigation under room temperature (R.T., 22 ± 5 °C). As shown in Table S2, when the H_2/CO ratio was controlled by the $Ni_{0.20}Co_{0.80}$@NCNT catalyst, the cascaded system maintained a high phenylacetylene conversion efficiency of 87% at R.T. Notably, the aldehyde selectivity increased to ca. 53%, with product yields of 31% for **b**, 11% for **c**, and 4% for **cH** (Fig. 4D). Furthermore, we conducted phenylacetylene hydroformylation reactions directly using syngas with different H_2/CO molar ratios ranging from 0.50 to 1.85 as reactants (Table S3), where the phenylacetylene conversion maintained over 90%, while the aldehyde selectivity was over 60%. Thus, a H_2/CO molar ratio between 0.50 and 1.85 is considered suitable for phenylacetylene hydroformylation. These results manifest the feasibility of integrating the eCO_2RR with hydroformylation process to synthesize valuable high-carbon aldehydes from CO_2.

In conclusion, by tuning the current density and Ni content in Ni_xCo_{1-x}@NCNT catalysts, we successfully accomplish the modulation of H_2/CO ratio from 0 to 5.3 during the eCO_2RR process. Syngas with a suitable H_2/CO ratio is obtained using the $Ni_{0.20}Co_{0.80}$@NCNT catalyst. The syngas is subsequently employed in the phenylacetylene hydroformylation reaction, catalyzed by Rh catalysts modified with indolybiphosphoramidite ligands. The tandem system achieves a high phenylacetylene conversion efficiency of 87%, with aldehyde selectivity reaching up to ca. 53% under ambient temperature and pressure. This work provides a new thought for upgrading CO_2 into valuable products.

This work is financially supported by the National Natural Science Foundation of China (22575158), China Scholarship Council, Sichuan Provincial Natural Science Foundation (2024YFFK0016, 2024ZYD0099) and the Fundamental Research Funds for the Central Universities (20822041J4097, 0082604151502). We thank Feng Yang, Jing Li, Yue Qi, and Dongyan Deng from the Comprehensive Training Platform of the Specialized Laboratory in the College of Chemistry, as well as Li Wu and Xiaobin Xie at Analytical & Testing Center of Sichuan University for compound testing.

Conflicts of interest

There are no conflicts to declare.

Data availability

All data supporting the findings of this study are available within the article and its electronic supplementary materials (ESI).

Notes and references

1 J. Ye, N. Dimitratos, L. M. Rossi, N. Thonemann, A. M. Beale and R. Wojcieszak, *Science*, 2025, **387**, eadn9388.

2 (a) S. Nitopi, E. Bertheussen, S. B. Scott, X. Liu, A. K. Engstfeld, S. Horch, B. Seger, I. E. L. Stephens, K. Chan, C. Hahn, J. K. Nørskov, T. F. Jaramillo and I. Chorkendorff, *Chem. Rev.*, 2019, **119**, 7610–7672. (b) S. Jia, X. Ma, X. Sun and B. Han, *CCS Chem.*, 2022, **4**, 3213–3229.

3 (a) S. Wang, P. Wang, D. Shi, S. He, L. Zhang, W. Yan, Z. Qin, J. Li, M. Dong, J. Wang, U. Olsbye and W. Fan, *ACS Catal.*, 2020, **10**, 2046–2059. (b) Y. Xu and M. Ding, *Chem. Soc. Rev.*, 2025, **54**, 2881–2905.

4 (a) D. M. Hood, R. A. Johnson, A. E. Carpenter, J. M. Younker, D. J. Vinyard and G. G. Stanley, *Science*, 2020, **367**, 542–548. (b) Y. Xu, W. Liu, Z. Xu, Y. Zhou and X.-Y. Yu, *Chem. Commun.*, 2023, **59**, 8596–8599. (c) M. Xu, D. Yang, H. Fang, Z. Sun, S. Tao, S. Yang, R. Li, H. Chen, C. Cheng, X. Wang, T. Ma and X. Zheng, *J. Catal.*, 2025, **443**, 115977. (d) H. Fang, Z. Sun, M. Xu, W. Xue, Z. Qian, Z. Li, C. Zhang, Q. Wu, J. Xu, R. Li, H. Fu, X. Zheng and H. Chen, *Ind. Eng. Chem. Res.*, 2025, **64**, 1488–1496. (e) P. Wang, F.-K. Chiang, J. Chai, A. I. Dugulan, J. Dong, W. Chen, R. J. P. Broos, B. Feng, Y. Song, Y. Lv, Q. Lin, R. Wang, I. A. W. Filot, Z. Men and E. J. M. Hensen, *Nature*, 2024, **635**, 102–107. (f) J. Zhao, X. Zheng, S. Tao, Y. Zhu, J. Yi, S. Tang, R. Li, H. Chen, H. Fu and M. Yuan, *Org. Lett.*, 2021, **23**, 6067–6072.

5 (a) T. Liu, H. Luo, T. Ouyang and Z.-Q. Liu, *Adv. Funct. Mater.*, 2025, **35**, 2415367. (b) Y. Chen, M. Xia, C. Zhou, Y. Zhang, C. Zhou, F. Xu, B. Feng, X. Wang, L. Yang, Z. Hu and Q. Wu, *ACS Nano*, 2023, **17**, 22095–22105. (c) Y. Ji, Y. Shi, C. Liu and B. Zhang, *Sci. China Mater.*, 2020, **63**, 2351–2357. (d) S. Wei, J. Zhu, X. Chen, R. Yang, K. Gu, L. Li, C.-Y. Chiang, L. Mai and S. Chen, *Nat. Commun.*, 2025, **16**, 1652.

6 (a) S. Wang, S. Zhou, Z. Ma, N. Gao, R. Daiyan, J. Leverett, Y. Shan, X. Zhu, Y. Zhao, Q. Liu, R. Amal, X. Lu, T. Liu, M. Antonietti, Y. Chen, Q. Zhang and Z. Tian, *Angew. Chem. Int. Ed.*, 2025, **64**, e202501896. (b) S. Lv, X. Sun, B. Wang, W. Wan, L. Wang, J. Wang and J. Zhang, *Adv. Sci.*, 2025, e05424. (c) Z. Chen, D. Zuo, L. Zhao, Y. Chen, F. Sun, L. Wang, H. Shen and Q. Tang, *Chem. Sci.*, 2025, **16**, 10397–10413.

7 (a) J. Zhang, X. Kang, Y. Yan, X. Ding, L. He and Y. Li, *Angew. Chem. Int. Ed.*, 2024, **63**, e202315777. (b) A. N. Biswas, Z. Xie, R. Xia, S. Overa, F. Jiao and J. G. Chen, *ACS Energy Lett.*, 2022, **7**, 2904–2910.

8 (a) Y. Jia, X. Xiong, D. Wang, X. Duan, K. Sun, Y. Li, L. Zheng, W. Lin, M. Dong, G. Zhang, W. Liu and X. Sun, *Nano-Micro Lett.*, 2020, **12**, 116. (b) Q. Qin, H. Jang, L. Chen, G. Nam, X. Liu and J. Cho, *Adv. Energy Mater.*, 2018, **8**, 1801478. (c) L. Chai, W. Yuan, X. Cui, H. Jiang, J. Tang and X. Guo, *RSC Adv.*, 2018, **8**, 26871–26879. (d) J. Zhang, H. Jang, L. chen, X. Jiang, M. G. Kim, Z. Wu, X. Liu and J. Cho, *Mater. Chem. Phys.*, 2020, **241**, 122375.

9 (a) J. Li, X. Li, M. Li, Q. Jiang, J. Liu, R. Duan, G. Cao, J. Wang and W. Li, *Chem. Commun.*, 2024, **60**, 14479–14482. (b) G. Jia, Y. Sun, P. Liu, J. Luo, P. Zhang, Y. Wei, W. Song, Z. Li, Z. Zhao and J. Liu, *Nano Res.*, 2025, **18**, 94907265.

10 (a) B. Zhang, J. Zou, Z. Chen, W. Yan, W. Liu, C. Dong, D. Cai, Q. Zhang, Y. Wang and S. Xie, *Next Nanotechnol.*, 2023, **2**, 100014. (b) Z. Wang, Y. Zhou, D. Liu, R. Qi, C. Xia, M. Li, B. You and B. Y. Xia, *Angew. Chem. Int. Ed.*, 2022, **61**, e202200552.

11 (a) J. Li, R. Wang, L. Han, T. Wang, Y. Asakura, C. Wang, G. Wang, X. Xu and Y. Yamauchi, *Nat. Commun.*, 2025, **16**, 1996. (b) B. Li, X. Sun and D. Su, *Phys. Chem. Chem. Phys.*, 2015, **17**, 6691–6694.

12 A. Ashok, A. Kumar, J. Ponraj and S. A. Mansour, *Carbon*, 2020, **170**, 452–463.

13 Q. He, D. Liu, J. H. Lee, Y. Liu, Z. Xie, S. Hwang, S. Kattel, L. Song and J. G. Chen, *Angew. Chem. Int. Ed.*, 2020, **59**, 3033–3037.

14 J. A. Rabinowitz and M. W. Kanan, *Nat. Commun.*, 2020, **11**, 5231.

View Article Online
DOI: 10.1039/D5CC04457J

Data Availability Statement

All data supporting the findings of this study are available within the article and its electronic supplementary materials (ESI).